

# Morphology changes in the evolution of liquid two-layer films

Andrey Pototsky, Michael Bestehorn, and Domnic Merkt

*Lehrstuhl für Theoretische Physik II,  
Brandenburgische Technische Universität Cottbus,  
Erich-Weinert-Straße 1, D-03046 Cottbus, Germany*

Uwe Thiele

*Max-Planck-Institut für Physik komplexer Systeme,  
Nöthnitzer Straße 38, D-01187 Dresden, Germany*

## Abstract

We consider two thin layers of immiscible liquids on a heated solid horizontal substrate. The free liquid-liquid and liquid-gas interfaces of such a two-layer (or bilayer) liquid film may be unstable due to effective molecular interactions or the Marangoni effect. Using a long wave approximation we derive coupled evolution equations for the interface profiles for a general non-isothermal situation allowing for slip at the substrate. Linear and nonlinear analyses are performed for isothermal ultrathin layers below 100 nm thickness under the influence of destabilizing long-range and stabilizing short-range interactions. Flat films may be unstable to varicose, zigzag or mixed modes. During the long-time evolution the nonlinear mode type can change via switching between two different branches of stable stationary solutions or via coarsening along a single such branch.

PACS numbers: 68.15.+e, 81.16.Rf, 68.55.-a, 47.20.Ky

## I. INTRODUCTION.

Instability phenomena in liquid films with a free liquid-gas interface on a solid support have attracted much interest recently. A long-wave or lubrication approximation [1, 2, 3, 4] is used as a very powerful tool for studying the behavior of relatively thin films and flows with small Reynolds numbers  $\text{Re} \lesssim 1$ . The behavior of one-layer liquid films is well understood in the different thickness ranges. There exist several mechanisms, driven by forces of different nature, which can destabilize an initially flat film on a solid substrate. They are investigated in a large number of theoretical [4, 5, 6, 7, 8, 9, 10, 11, 12, 13, 14, 15, 16, 17, 18, 19] and experimental [20, 21, 22, 23, 24, 25] works. For film thicknesses  $d$  less than about 100 nm, effective intermolecular interactions between the film surface and the substrate dominate all the other forces, like thermo- and soluto-capillarity or gravity, and thus determine the film stability. For film thicknesses above 100 nm, eventually the thermocapillary forces become important. If the film is heated from the substrate the flat liquid-gas interface may become unstable due to large-scale Marangoni convection [23, 26]. It is dominant up to an upper border for the film thickness determined by the competition between the large-scale and the small-scale convection mode [27]. For thicker films with  $d \geq 100 \mu\text{m}$  also gravity becomes important allowing for the Rayleigh-Taylor instability to occur [5, 6].

One can estimate the upper limit for the film thickness range where lubrication approximation is valid by comparing the wave length of the dominant instability mode  $\lambda_m$  and the film thickness  $d$ . For the Rayleigh-Taylor instability the wave length  $\lambda_m$  depends on the interfacial tension, the density of the liquid and the gravitational acceleration. It does not depend on the film thickness [4] and is of the order of  $10^3$  to  $10^4 \mu\text{m}$ . This implies that the film thickness should be smaller than  $10^2$  to  $10^3 \mu\text{m}$  to satisfy the condition for the validity of the lubrication approximation, i.e.  $d/\lambda \ll 1$ .

In the following we focus on the stability and evolution of liquid films with thicknesses below 100 nm [11, 24, 28, 29]. Such films become unstable if the energy of the intermolecular interaction has a negative second derivative with respect to the film thickness. For films with thicknesses above 10 nm only the long-range Van der Waals forces are relevant. They can be of different nature depending on the molecular properties of the involved media. One distinguishes interactions between two randomly orienting dipoles (orientation interaction), between a randomly orienting dipole and an induced dipole (induction interaction) and

between a fluctuating dipole and an induced dipole (dispersion interaction). Between two parallel interfaces at a distance  $h$ , the sum of these forces decays as  $A/h^3$ , where  $A$  is the Hamaker constant [30]. An unstable situation corresponds to a positive Hamaker constant. The intrinsic wave length of the instability  $\lambda$  increases monotonically with  $d$  as  $\lambda \sim d^2$  [4]. The stability of a flat film may change dramatically, if the substrate is coated with a layer of different dielectric properties as, for instance, a silicon substrate (Si) coated with an silicon oxide layer (SiO) [31]. In the latter case, for an oxide layer of about 2 nm only ultrathin film below about 4 nm are linearly unstable. Increasing the film thickness in the linearly unstable range, the wave length  $\lambda$  increases rapidly and diverges at stabilization at the critical thickness  $d_c$ . Above  $d_c$  the flat film is linearly stable.

Imagine we interchange the solid coating by a second liquid layer. Then the stability of the (now) upper layer will still depend on the (now liquid) coating layer. However, additionally the liquid coating layer itself may be unstable. This situation leads quite naturally to the extension of the well studied one-layer systems to two-layer systems. In general, there exist two possible geometries for such systems. For two liquid layers inbetween two solid plates only the interface between the two liquids is free to move, i.e. the situation can be described by a single evolution equation [32, 33, 34]. For two liquid layers on a substrate below a gas atmosphere both interfaces, the liquid-liquid and the liquid-gas one, are free to move. Their evolution has to be described by coupled evolutions [35, 36, 37, 38, 39, 40, 41, 42, 43].

The experimental interest in two-layer liquid films is mainly focused on the dewetting of a liquid layer from a liquid bulk substrate or from a thick liquid layer [44, 45, 46, 47, 48, 49].

The dewetting of a polystyrene (PS) layer of 15 to 68 nm thickness from a highly viscous, 46 nm thick polyamide (PA) layer is investigated in Ref. [44]. The PA layer was spin-coated onto a native oxide covered silicon (Si) wafer. At high temperature (195°C) and small thicknesses (15...35 nm) the PS layer is unstable and dewets exhibiting typical spinodal patterns. To the contrary, at low temperature (115°C), when the PA layer is solid, the PS layer is stable, independent of its thickness.

Relatively thick layers with thicknesses between 100 nm and 1  $\mu$ m are metastable and may dewet by nucleation of holes, as was shown in Ref. [50] for poly(dimethylsiloxane) (PDMS) layers deposited on a fluorinated PDMS substrate. The velocity of the growth of holes was found to be inversely proportional to the substrate viscosity and its thickness. For polystyrene (PS) films on a poly(methylmethacrylate) (PMMA) substrate, both with thick-

nesses of about 100 nm, the dewetting velocity was found to exhibit a minimum as a function of PMMA viscosity [48]. Furthermore, for a polycarbonate (PC) film on a poly(styrene-*co*-acrylonitrile) (SAN) substrate Ref. [49] reports a non-trivial dependence of the dewetting velocity on both, the film thickness and the thickness of the substrate.

Recently we shortly introduced coupled evolution equations for two-layer liquid films taking into account long-range Van der Waals interactions only [40]. This allows to study pathways towards rupture but can not describe the long-time evolution of such films. In the present paper we study the short- and long-time evolution of two-layer liquid films incorporating long-range and short-range interactions. Thereby the main focus lies again on ultrathin layers with respective thicknesses below 100 nm for which the effective molecular interactions between the four media are the dominant influences. However, in Section II A the governing evolution equations are derived for the more general non-isothermal case.

Section III A presents the linear stability analysis for the isothermal case. We discuss the possibility to destabilize flat films by changing the mean layer thicknesses in Section III B and two possible mode types in Section III C. In Section III D the linear stability is considered for two important limiting cases of a vanishing upper and of a vanishing lower layer. In Section IV we investigate the non-uniform stationary solutions and their stability. Two different pathways for a mode-change are predicted. In Section V A the time simulations of the non-linear evolution equations are presented. The change of the surface morphology via switching between a varicose and a zigzag mode is demonstrated. The long-time stationary solutions are discussed for different experimentally studied systems in Section V B.

## II. DERIVATION OF COUPLED LARGE-AMPLITUDE EVOLUTION EQUATIONS

### A. General case

First, we derive coupled evolution equations for the profile of the liquid-liquid interface  $h_1(x, y)$  and the one of the liquid-gas interface  $h_2(x, y)$ . Considering a two-dimensional geometry as sketched in Fig. 1 the Stokes equations for the two layers write

$$\nabla(p_i + \phi_i) = \mu_i \Delta \vec{v}_i, \quad (1)$$

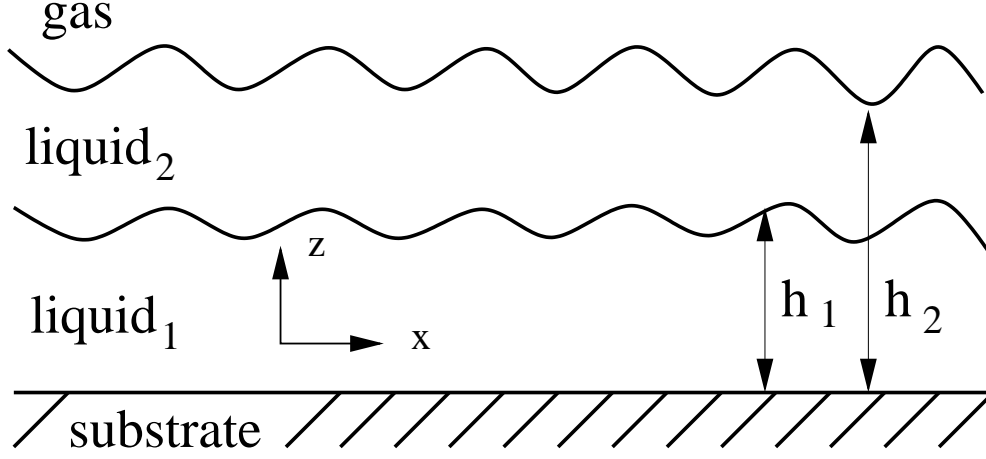


FIG. 1: Sketch of the problem in two dimensions. The local thickness of the lower layer is  $h_1$ , the total local film thickness is  $h_2$ . Due to the conservation of mass the mean thicknesses do not change with time, i.e.  $d_1 = \int h_1 dx$  and  $d_2 = \int h_2 dx$ .

where  $i = 1, 2$  denotes the respective layer. For each layer  $\vec{v}_i = (u_i, w_i)$  is the velocity field,  $p_i$  the pressure,  $\phi_i$  the potential of the bulk forces and  $\mu_i$  the viscosity. The lubrication approximation [4] is applied assuming the ratio of vertical and horizontal length scales to be small. We use as smallness parameter the ratio  $\epsilon = d_1/\lambda$  where  $\lambda$  is the characteristic lateral length scale of the film instability. In zeroth order in  $d_1/\lambda$  the Stokes equations (1) simplify to

$$\mu_2 \partial_z^2 u_2 = \partial_x \bar{p}_2 \quad (2)$$

$$\partial_z \bar{p}_2 = 0 \quad (3)$$

$$\mu_1 \partial_z^2 u_1 = \partial_x \bar{p}_1 \quad (4)$$

$$\partial_z \bar{p}_1 = 0, \quad (5)$$

where the  $\bar{p}_i$  stand for  $p_i + \phi_i$ . At the substrate ( $z = 0$ ) we use a Navier slip condition and non-penetration, i.e.

$$u_1 = \beta \partial_z u_1 \quad \text{and} \quad w_1 = 0 \quad (6)$$

where  $\beta$  is the slip length. At the liquid-liquid interface ( $z = h_1$ ) we use the continuity of the velocity field, the kinematic condition and the continuity of the tangential component

of the liquid stress tensor

$$u_1 = u_2, \quad w_1 = w_2, \quad (7)$$

$$w_1 = \partial_t h_1 + u_1 \partial_x h_1, \quad (8)$$

$$(9)$$

and

$$\mu_1 \partial_z u_1 - \mu_2 \partial_z u_2 = \partial_x \sigma_{12}, \quad (10)$$

respectively. The normal stress condition is discussed below. At the liquid-gas interface ( $z = h_2$ ) only the kinematic condition and the continuity of the tangential component of the liquid stress tensor are applied

$$w_2 = \partial_t h_2 + u_2 \partial_x h_2 \quad (11)$$

$$\mu_2 \partial_z u_2 = \partial_x \sigma_2. \quad (12)$$

The  $\sigma_{12}$  and  $\sigma_2$  stand for the interfacial tensions of the liquid-liquid and of the liquid-gas interface, respectively.

The boundary conditions for the normal component of the stress tensor are written incorporating the disjoining pressures at the liquid-liquid  $\Pi_1(h_1, h_2)$  and at the liquid-gas  $\Pi_2(h_1, h_2)$  interface, respectively. The disjoining pressures represent effective molecular interactions between the interfaces that result, for instance, from Van der Waals interactions [51]. They are discussed in detail below. This gives for the liquid-gas interface ( $z = h_2$ )

$$p_2(h_2) - p_0 = -\sigma_2 \partial_x^2 h_2 + \Pi_2(h_1, h_2)$$

and for the liquid-liquid interface ( $z = h_1$ )

$$p_1(h_1) - p_2(h_1) = -\sigma_{12} \partial_x^2 h_1 + \Pi_1(h_1, h_2), \quad (13)$$

where  $p_0$  is the constant pressure in the gas layer. As a consequence there are pressure jumps at the interfaces.

Eqs. (13) can be written in terms of variations of an energy functional  $F[h_1, h_2]$

$$\begin{aligned} p_1(h_1) - p_2(h_1) &= \frac{\delta F}{\delta h_1} \\ p_2(h_2) - p_0 &= \frac{\delta F}{\delta h_2}, \end{aligned} \quad (14)$$

with

$$F = \int \left( \sigma_1 \frac{(\partial_x h_1)^2}{2} + \sigma_2 \frac{(\partial_x h_2)^2}{2} + f(h_1, h_2) \right) dx, \quad (15)$$

and  $f(h_1, h_2)$  the free energy of the flat films per unit area.

Equations (2) and (4) are integrated three times with respect to  $z$  to obtain the stream functions  $\Psi_i$ , defined by ( $w_i = -\partial_x \Psi_i$ ,  $u_i = \partial_z \Psi_i$ ). The six  $x$ -dependend integration constants are determined using the boundary conditions (6), (7), (10), and (12). Thus the velocity fields in the two layers are given by

$$\begin{aligned} u_1 &= \frac{1}{\mu_1} (\partial_x \bar{p}_1) \frac{z^2}{2} + \frac{1}{\mu_1} (z + \beta) K_1 \\ u_2 &= \frac{1}{\mu_2} (\partial_x \bar{p}_2) \frac{z^2}{2} + \frac{1}{\mu_2} K_2 (z - h_1) - \frac{\partial_x \bar{p}_2}{\mu_2} \frac{h_1^2}{2} + u_1(h_1), \end{aligned} \quad (16)$$

with  $K_1 = K_2 + \partial_x \sigma_{12} + [(\partial_x \bar{p}_2) - (\partial_x \bar{p}_1)] h_1$  and  $K_2 = \partial_x \sigma_2 - (\partial_x \bar{p}_2) h_2$ .

The stream functions  $\Psi_i$  are related to the flows in the lower  $\Gamma_1 = \int_0^{h_1} u_1 dz$  and in the upper layer  $\Gamma_2 = \int_{h_1}^{h_2} u_2 dz$  by  $\Gamma_1 = \Psi_1(h_1)$ ,  $\Gamma_1 + \Gamma_2 = \Psi_2(h_2)$ . Using the  $\Psi_i$  we rewrite Eqs. (8) and (11) to obtain the evolution equations of the two interfaces

$$\partial_t h_1 + \partial_x [\Psi_1(h_1)] = 0 \quad (17)$$

$$\partial_t h_2 + \partial_x [\Psi_2(h_2)] = 0. \quad (18)$$

Written in terms of the energy functional they read

$$\begin{aligned} \partial_t h_1 &= \partial_x \left[ Q_{11} \partial_x \frac{\delta F}{\delta h_1} + Q_{12} \partial_x \frac{\delta F}{\delta h_2} - D_{11} \partial_x \sigma_{12} - D_{12} \partial_x \sigma_2 \right] \\ \partial_t h_2 &= \partial_x \left[ Q_{21} \partial_x \frac{\delta F}{\delta h_1} + Q_{22} \partial_x \frac{\delta F}{\delta h_2} - D_{21} \partial_x \sigma_{12} - D_{22} \partial_x \sigma_2 \right], \end{aligned} \quad (19)$$

with the mobility matrices of the pressure terms

$$\mathbf{Q} = \frac{1}{\mu_1} \begin{pmatrix} \frac{h_1^3}{3} + \beta h_1^2 & \frac{h_1^2}{2} (h_2 - \frac{h_1}{3}) + \beta h_1 h_2 \\ \frac{h_1^2}{2} (h_2 - \frac{h_1}{3}) + \beta h_1 h_2 & \frac{(h_2 - h_1)^3}{3} (\frac{\mu_1}{\mu_2} - 1) + \frac{h_2^3}{3} + \beta h_2^2 \end{pmatrix} \quad (20)$$

and of the tangential stress terms

$$\mathbf{D} = \frac{1}{\mu_1} \begin{pmatrix} \frac{h_1^2}{2} + \beta h_1 & \frac{h_1^2}{2} + \beta h_1 \\ h_1 (h_2 - \frac{h_1}{2}) + \beta h_2 & \frac{\mu_1 (h_2 - h_1)^2}{2\mu_2} + h_1 (h_2 - \frac{h_1}{2}) + \beta h_2 \end{pmatrix}, \quad (21)$$

respectively. Note, that the mobility matrix  $\mathbf{Q}$  is symmetric and all mobilities  $Q_{ik}$  and  $D_{ik}$  are positive. Note that the Eqs. (19) without the effective molecular interactions represent

the fully nonlinear equivalent for the weakly nonlinear equations derived in Ref. [52, 53]. Assuming that the interfacial tensions are influenced by thermocapillarity only, one can express the derivatives  $\partial_x \sigma_{12}$  and  $\partial_x \sigma_2$  in terms of gradients of local thicknesses  $\partial_x h_i$ . This is done in the VII.

For isothermal ultrathin liquid films ( $\partial_x \sigma_{12} = \partial_x \sigma_2 = 0$ ), the situation is relaxational (or variational), i.e. the Eqs. (19) possess a Lyapunov functional, namely the energy functional  $F$ , which decreases monotonously in time as shown next. The total time derivative of the Lyapunov functional is  $dF/dt = \int \left( \frac{\delta F}{\delta h_1} \partial_t h_1 + \frac{\delta F}{\delta h_2} \partial_t h_2 \right) dx$ . Expressing  $\partial_t h_i$  by Eqs. (19) and using partial integration with periodic boundary conditions, one obtains

$$\frac{dF}{dt} = - \int \sum_{i,k} Q_{ik} \left( \partial_x \frac{\delta F}{\delta h_i} \right) \left( \partial_x \frac{\delta F}{\delta h_k} \right) dx. \quad (22)$$

Because

$$\det \mathbf{Q} = \frac{(h_2 - h_1)^3 h_1^3}{9\mu_1 \mu_2} + \frac{1}{12\mu_1^2} h_1^4 (h_2 - h_1)^2 + \beta \left( \frac{h_1^3}{3\mu_1^2} (h_2 - h_1)^2 + h_1^2 \frac{(h_2 - h_1)^3}{3\mu_1 \mu_2} \right) > 0 \quad (23)$$

and  $Q_{ii} > 0$ , the quadratic form in Eq. (22) is positive definite implying  $dF/dt < 0$ . The existence of  $F$  allows to identify the stationary solutions of Eqs. 19 with the extrema of  $F$ . This will be used in Section IV.

## B. Driving forces, specification of $\Pi(h_1, h_2)$

In many important cases, as for instance, for polymer films on apolar substrates [20, 24], the interaction energy is mainly determined by its long-range apolar dispersion part. However, if only a destabilizing long-range interaction is taken into account in the model the time evolution ends with the rupture of the upper or lower layer [40]. To prevent film rupture we also take here into account stabilizing short-range interactions [14, 51]. The latter are normally not relevant for films of thicknesses above 100 nm and thus do not change the stability of corresponding flat films. For layers thicker than about 10 nm the short-range part becomes important in the non-linear stage of evolution when the local thicknesses becomes comparable to its interaction length.

The long-range part of the interaction energy between each pair of interfaces from Fig. 1, is represented by the dispersive Van der Waals interaction and given by  $A_{ijkl}/2\pi h^2$  [51], where  $A_{ijkl}$  is the dispersive (four-index) Hamaker constant which corresponds to the interaction



between the interfaces  $i-j$  and  $k-l$  and  $h$  is the distance between the interfaces. Each index in  $A_{ijkl}$  can be one of the following four letters  $g, 2, 1$  and  $s$ , denoting the gas layer, liquid 2, liquid 1 and the substrate, respectively. The four-index Hamaker constant is calculated using an equivalent of Eq. (11.13) of Ref. [51] that is based on the assumption that the main absorption frequencies of all involved media are about  $\nu = 3 \times 10^{15}$  Hz and that the zero frequency contribution is negligible. This yields

$$A_{ijkl} \approx \frac{3h\nu_e}{8\sqrt{2}} \frac{(n_i^2 - n_j^2)(n_l^2 - n_k^2)}{(n_i^2 + n_j^2)^{1/2}(n_l^2 + n_k^2)^{1/2}[(n_i^2 + n_j^2)^{1/2} + (n_l^2 + n_k^2)^{1/2}]}, \quad (24)$$

where  $n_i$  are the refractive indices of the media. The three-index Hamaker constants are obtained using

$$A_{ijk} = A_{ijjk}. \quad (25)$$

The short-range forces which can be of a electrostatic or structural nature [54, 55] decay exponentially with  $h$ . The electrostatic part results from the formation of diffuse electric double-layers in the vicinity of the interfaces of polar liquids [56, 57, 58]. For small film thicknesses the diffuse double-layers at the two interfaces overlap resulting in a repulsive or attractive force between the interfaces. The corresponding interaction energy between the interfaces  $s-1$  and  $1-2$  is given by  $S_1 \exp[(l_0 - h_1)/l_1]$  and between the interfaces  $1-2$  and  $2-g$  by  $S_2 \exp[(l_0 - (h_2 - h_1))/l_2]$ , where  $l_0 = 0.158$  nm is the Born repulsion length,  $l_1, l_2 \sim 1..10$  nm are the interaction lengths of the short-range interactions [14]. Further on we consider the two correlation lengths  $l_1$  and  $l_2$  to be equal and denote them by  $l$ .  $S_1 > 0$  and  $S_2 > 0$  are the short-range components of the total spreading coefficients, related to the lower layer on the substrate below a bulk of the upper liquid and to the upper layer on the lower film below the ambient gas, respectively. We do not take into account short-range interaction between interfaces  $s-1$  and  $2-g$ .

Collecting the long-range and the short-range forces the disjoining pressures  $\Pi_1(h_1, h_2)$  and  $\Pi_2(h_1, h_2)$  are specified as

$$\begin{aligned} \Pi_1(h_1, h_2) &= \frac{A_{21s}}{6\pi h_1^3} - \frac{A_{12g}}{6\pi(h_2 - h_1)^3} - \frac{S_1}{l_1} \exp\left[\frac{l_0 - h_1}{l_1}\right] + \frac{S_2}{l_2} \exp\left[\frac{l_0 - (h_2 - h_1)}{l_2}\right] \\ \Pi_2(h_1, h_2) &= \frac{A_{12g}}{6\pi(h_2 - h_1)^3} + \frac{A_{g21s}}{6\pi h_2^3} - \frac{S_2}{l_2} \exp\left[\frac{l_0 - (h_2 - h_1)}{l_2}\right] \end{aligned} \quad (26)$$

To non-dimensionalize Eqs.(19) we scale the thicknesses with  $l$ ,  $x$  with  $\lambda = l(d_2 - d_1)\sqrt{2\pi\sigma_1/|A_{12g}|}$ , and  $t$  with  $\tau = (2\pi)^2\sigma_1\mu_1 l(d_2 - d_1)^4/A_{12g}^2$ . Then the scaled energy func-

tional reads:

$$F = \int \left[ \frac{1}{2}(\partial_x h_1)^2 + \frac{\sigma}{2}(\partial_x h_2)^2 - \frac{\bar{A}_{12g}}{6(h_2 - h_1)^2} - \frac{\bar{A}_{21s}}{6h_1^2} - \frac{\bar{A}_{g21s}}{6h_2^2} \right. \\ \left. + c_1(h_1 - \bar{d}_1) + c_2(h_2 - \bar{d}_2) + \bar{S}_1 \exp(-h_1) + \bar{S}_2 \exp(h_1 - h_2) \right] dx, \quad (27)$$

with the scaled Hamaker constants  $\bar{A}_{ijkl} = [(d_2 - d_1)/l]^2 A_{ijkl}/|A_{12g}|$ , spreading coefficients  $\bar{S}_i = 2\pi [(d_2 - d_1)]^2 S_i \exp(d_0/l)/|A_{12g}|$ , and mean layer thicknesses  $\bar{d}_i = d_i/l$ . The  $c_i$  are Lagrange multipliers that ensure mass conservation for the two liquids. The corresponding energy scale is  $|A_{12g}|/2\pi(d_2 - d_1)^2$ . The ratios of the mean layer thicknesses, surface tensions and viscosities are  $d = d_2/d_1$ ,  $\sigma = \sigma_2/\sigma_1$  and  $\mu = \mu_2/\mu_1$ , respectively. Further on, we denote the scaled variables using the same symbols as before, i.e. the scaled mean thicknesses will be denoted by  $d_i$  and the local thicknesses by  $h_i$ . The non-dimensional mobility matrices are obtained from Eqs. (20) and (21) by dropping the factor  $1/\mu_1$  and replacing  $\beta$  by  $\beta/l$ .

### III. LINEAR STABILITY

#### A. General stability of flat films

We start the analysis of our model for two-layer films by discussing the linear stability of flat films with  $h_1(x) = d_1$  and  $h_2(x) = d_2$ . We linearize Eqs. (19) in  $\epsilon \ll 1$  for small amplitude disturbances  $\epsilon \chi_i \exp(\gamma t) \exp(kx)$  for  $i = 1, 2$  where  $k$ ,  $\gamma$  and  $\chi = (\chi, 1)$  are the wave number, growth rate and amplitudes of the disturbance, respectively. The dispersion relation  $\gamma(k)$  is obtained solving the resulting eigenvalue problem  $(\mathbf{J} - \gamma \mathbf{I})\chi = 0$ .

For the isothermal case ( $\partial_x \sigma_{12} = \partial_x \sigma_2 = 0$  in Eqs. (19)), the corresponding *non*-symmetric Jacobi matrix  $\mathbf{J}$  is given by  $\mathbf{J} = -k^2 \mathbf{Q} \cdot \mathbf{E}$ , where  $\mathbf{Q}$  is the scaled mobility matrix and  $\mathbf{E}$  is the energy matrix

$$\mathbf{E} = \begin{pmatrix} \frac{\partial^2 f}{\partial h_1^2} + k^2 & \frac{\partial^2 f}{\partial h_1 \partial h_2} \\ \frac{\partial^2 f}{\partial h_1 \partial h_2} & \frac{\partial^2 f}{\partial h_2^2} + \sigma k^2 \end{pmatrix}, \quad (28)$$

where  $f(h_1, h_2)$  is the local part of the energy density from Eq. (27). This yields

$$\gamma = \frac{\text{Tr}}{2} \pm \sqrt{\frac{\text{Tr}^2}{4} - \text{Det}}, \quad (29)$$

where  $\text{Tr} = -k^2[2Q_{12}E_{12} + Q_{11}E_{11} + Q_{22}E_{22}]$  and  $\text{Det} = k^4 \det \mathbf{Q} \det \mathbf{E}$  are the trace and the determinant of  $\mathbf{J}$ . Since  $\det \mathbf{Q} \neq 0$  the eigenvalue problem can be written as

the generalized eigenvalue problem  $(k^2 \mathbf{E} + \gamma \mathbf{Q}^{-1}) \boldsymbol{\chi} = 0$ . Because  $\mathbf{E}$  and  $\mathbf{Q}^{-1}$  are both symmetric and  $\mathbf{Q}^{-1}$  is positive definite one can deduce that all eigenvalues  $\gamma$  are real [59] as expected for a variational problem. In the non-isothermal case, the Jacobi matrix is given by  $\mathbf{J} = -k^2(\mathbf{Q}\mathbf{E} - \mathbf{D}\mathbf{\Gamma})$ , where  $\mathbf{\Gamma}$  is the scaled matrix of coefficients before  $\partial_x h_i$ , defined in Section VII. Neither the matrix  $\mathbf{D}$  nor  $\mathbf{\Gamma}$  are symmetric. This leads to (in general) complex eigenvalues indicating the possibility of oscillating motion in the non-isothermal case [52, 53].

Going back to the isothermal case, inspection of the generalized eigenvalue problem shows that the stability threshold is completely determined by the eigenvalues of  $\mathbf{E}$  alone. Since the surface tension terms are always positive, the onset of an instability is always found for  $k = 0$ , i.e. the system is linearly stable, independently of the wavelength of the disturbance, for

$$\det \mathbf{E} > 0 \quad \text{and} \quad E_{11} > 0 \quad \text{at} \quad k = 0. \quad (30)$$

An instability sets in if at least one of the conditions (30) is violated. Then the flat two-layer film is unstable to disturbances with  $k$  larger zero and smaller than a cutoff wavenumber  $k_c$ . From Eq. (29) it follows that  $k_c$  is determined by  $\det \mathbf{E}(k_c) = 0$ , i.e.

$$k_c^2 = -\frac{1}{2} \left( \frac{\partial^2 f}{\partial h_1^2} + \frac{1}{\sigma} \frac{\partial^2 f}{\partial h_2^2} \right) \pm \sqrt{\frac{1}{4} \left( \frac{\partial^2 f}{\partial h_1^2} - \frac{1}{\sigma} \frac{\partial^2 f}{\partial h_2^2} \right)^2 + \frac{1}{\sigma} \left( \frac{\partial^2 f}{\partial h_1 \partial h_2} \right)^2}. \quad (31)$$

Fig. 2 shows a schematic stability diagram in the plane  $(E_{11}, E_{22})$ . The stability threshold  $E_{11}E_{22} = E_{12}^2$ ,  $E_{11} > 0$  is a hyperbole, represented by the solid line. The unstable region below and left of that line is divided by a second hyperbole into a two-mode and a one-mode region. In the two-mode region both growth rates given by Eq. (29) are positive for  $k$  smaller then the respective cut-off  $k_c$ . In the one-mode region only one  $\gamma$  is positive for  $k < k_c$ . Fixing all system parameters,  $\det \mathbf{E}(k)$  is determined by  $k$ . If at  $k = 0$  the system is in the two-mode region, then by increasing  $k$  one passes two times a line  $\det \mathbf{E} = 0$ , as indicated by the dashed arrow in Fig. 2. Each time one of the growth rates Eq. (29) crosses zero, i.e. the two modes are stabilized successively. If at  $k = 0$  the system is in the one-mode region the line  $\det \mathbf{E} = 0$  is crossed only once (dot-dashed line).

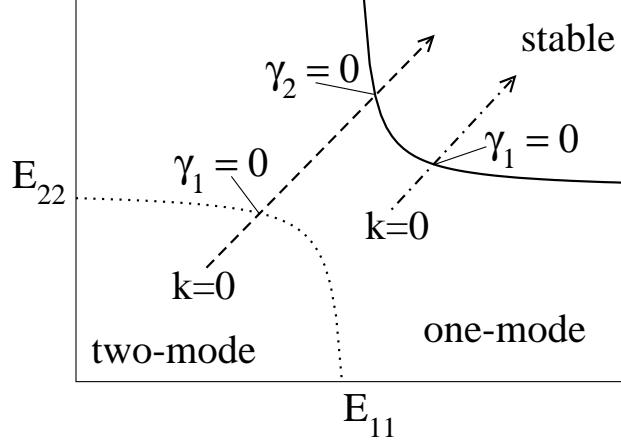


FIG. 2: The stability diagram for fixed coupling  $E_{12}$ . Shown are: the stability threshold (solid line), the boundary between the one-mode and the two-mode regions (dotted line). Dashed and dotted-dashed lines are the parametric lines:  $(E_{11}(k), E_{22}(k))$ . The dashed line has its start point in the two-mode region and the dotted-dashed in the one-mode region. In the points of intersections between the lines:  $\det \mathbf{E}(k=0)$  and the two parametric lines, one of the growth rates changes its sign.

### B. Long-range interaction only

As detailed above the stabilizing short-range interaction becomes important only if at least one local layer thicknesses is comparable to the interaction length  $l$ , i.e. if a layer becomes thinner than about 10 nm. Therefore, to study the linear stability of thicker layers one can neglect the short-range terms in Eq. (27).

In this case, Eq. (30) is used to study the role of the Hamaker constants Eq. (24) in the linear evolution of the system. First we note that the Hamaker constants are coupled through the refractive indices of the media  $n_i$ . This allows only for the selected combinations of signs of the  $A_{ijk}$  and  $A_{ijkl}$  that are given in Table I.

For fixed Hamaker constants, i.e. fixed combination of materials,  $\det \mathbf{E}_0 = \det \mathbf{E}(k=0)$  is only a function of the ratio  $d$  of the layer thicknesses. Using Table I one can show that for positive  $\partial^2 f / \partial h_i^2$  the equation  $\det \mathbf{E}_0(d) = 0$  can only have the solution  $d = 1$ , i.e.  $d_2 - d_1 = 0$ . This means that only for vanishing upper layer the system can be on the stability border. In consequence the stability threshold can *not* be crossed by solely changing the ratio of layer thicknesses. This was analyzed in Ref. [40] for a variety of experimentally studied systems.

refractive indices	$A_{12g}$	$A_{21s}$	$A_{g21s}$
$n_s > n_1, n_1 < n_2, n_2 > n_g$	+	+	-
$n_s < n_1, n_1 < n_2, n_2 > n_g$	+	-	+
$n_s < n_1, n_1 > n_2, n_2 > n_g$	-	+	+
$n_s > n_1, n_1 > n_2, n_2 > n_g$	-	-	-

TABLE I: Signs of the different Hamaker constants for given order of the refractive indices of the involved medias.

Increasing  $d$  from one the system remains either completely in the unstable or in the stable region.

To compare the stability of a two-layer film with that of a one-layer film we introduce two effective one-layer films as follows. For system (1) we assume the lower layer to be solid, i.e. we regard the upper layer as a one-layer film on a coated substrate. For system (2) we assume the upper layer to be rigid but deformable by bending (however, without bending energy). The lower liquid layer corresponds then to a one-layer film on a solid bulk substrate.

In case (1) the one-layer liquid film, is unstable if the second derivative of the energy with respect to the film thickness is negative  $\partial^2 f/h_2^2 < 0$ . The stability border  $\partial^2 f/h_2^2 = 0$  can be crossed by changing the layer thickness  $d_2 - d_1$  or the thickness of the coating layer  $d_1$ . This was demonstrated in Refs. [24, 60] for a PS film on Si wafers covered by a 1.6 nm thick SiO layer. The PS layers with thicknesses below 2.3 nm were found to be unstable. In case (2) the one-layer liquid film is unstable for  $\partial^2 f/h_1^2 < 0$ . It can also be destabilized by changing the layer thicknesses, as was shown in Ref. [61] for a rigid PS layer on top of a liquid PDMS layer on a Si substrate.

However, one notes in the stability diagram Fig. 2 that the stability threshold of the two-layer system lies in the region, where the both effective one-layer systems are stable. This indicates that the two-layer system is less stable than the corresponding effective one-layer systems.

### C. Different instability modes

The results presented up to here are general, but now we focus on selected two-layer films studied experimentally [48, 60, 62]. We consider various combinations of layers of polystyrene (PS), poly(methylmethacrylate) (PMMA) and poly(dimethylsiloxane) (PDMS) on a silicon (Si) or on a silicon-oxide (SiO) substrates. The Hamaker constants for different combinations are calculated using Eq. (24) and given in Table II.

System	$A_{12g} \times 10^{-20} \text{Nm}$	$A_{21s} \times 10^{-20} \text{Nm}$	$A_{g21s} \times 10^{-20} \text{Nm}$
Si/PMMA/PS/air	1.49	3.8	-23.02
SiO/PMMA/PS/air	1.49	-0.024	0.15
SiO/PS/PDMS/air	-1.83	0.42	1.25

TABLE II: Hamaker constants for various combinations of polymers.

The unstable mode can be of two different types. It can be a zigzag mode, i.e. the deflections of the two interfaces are in phase or a varicose mode, i.e. the deflections of the two interfaces are in anti-phase. Note, that the model in Ref. [35] neglects the interaction between the substrate and the liquid-liquid (liquid-gas) interface and therefore only finds an unstable varicose mode. In the general case, however, also the zigzag mode can become unstable. Both modes are normally asymmetric, i.e. the deflection amplitudes of the two interfaces differ. We characterize the asymmetry by  $\phi = \chi/(1 + \chi^2)$ . Negative (positive)  $\phi$  corresponds to varicose (zigzag) modes.  $\phi = 1/2$  is the most symmetric case, whereas  $\phi = 0$  corresponds to maximal asymmetry, i.e. one of the interfaces is flat. The asymmetry increases with the ratio of the surface tensions  $\sigma$ . Note, that the dispersion relation and the type of the dominant mode depend on  $\sigma$  and  $\mu$ , whereas the stability diagram Fig. 2 *does not*.

The two mode types are plotted in Fig. 3 for a Si/PMMA/PS/air system for a fixed value of  $d$  and different ratios of viscosities  $\mu$ . The dispersion relations  $\gamma(k)$  are shown together with the corresponding  $\phi$ .

We see that the type of the dominant mode can be changed by varying  $d$  or  $\mu$ . The change of mode types in dependence of the ratio of interfacial tensions  $\sigma$  is studied in Ref. [40].

Strictly speaking, the conception of the mode type, characterized by the angle  $\phi$  can only be used in the linear stage of the evolution. However to discuss morphology changes we

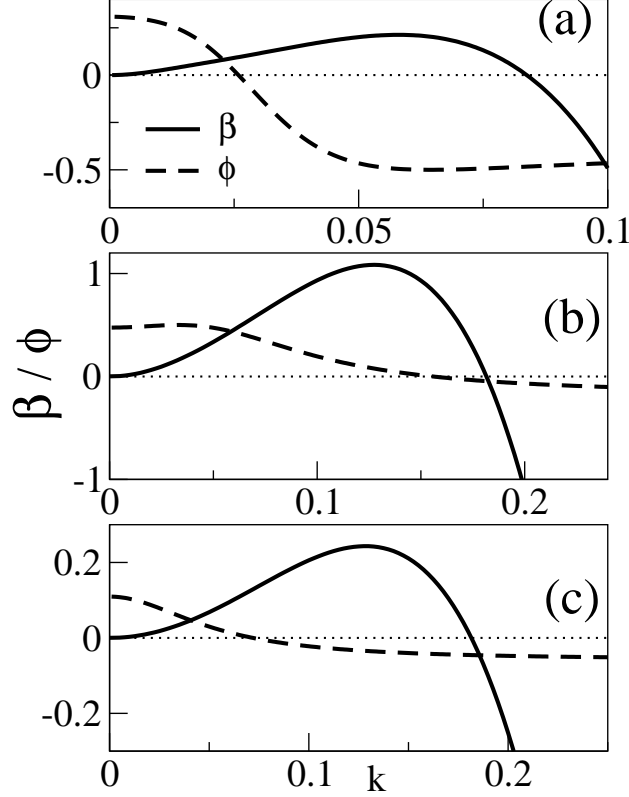


FIG. 3: Shown are the growth rate  $\gamma$  and the corresponding angle  $\phi$  of the leading eigenmode. An example for the one-mode varicose region in (a) for  $d_1 = 30$ ,  $d_2 = 47$  and in (b) the one-mode zigzag region at  $d_1 = 15$ ,  $d_2 = 40$  for parameters  $\sigma = \mu = 1$ . Panel (c) gives  $\beta$  and  $\phi$ , for the same mean thicknesses as in (b), but for  $\mu = 0.1$ . For convenience we plot  $10\gamma$  in (b) and  $20\gamma$  in (a).

generalize this concept to nonlinear thickness profiles  $h_i(x)$ . We define a generalized mode type by the integral

$$\phi_{\text{int}} = \frac{1}{L} \int \frac{(h_1 - d_1)(h_2 - d_2)}{[(h_1 - d_1)^2 + (h_2 - d_2)^2]} dx, \quad (32)$$

taken over the domain length  $L$ . As we will see in many cases the sign of the product  $(h_1 - d_1)(h_2 - d_2)$  does not depend on  $x$ . The generalized mode-type for this profiles coincides with the local one that can be determined by pure inspection of the profile by eyes. In the following we will use the notion "mode-type" also in the nonlinear regime.

#### D. Limiting cases

The radical in Eq. (29) does not allow to give an analytic expression for the fastest growing wave number  $k_m$  and its characteristic growth time  $\tau_m = 1/\gamma_m$  for general  $d_i$ . Nevertheless,

one can derive asymptotics for  $k_m$  and  $\tau_m$  in the two important limiting cases of (1) small thickness of the upper layer  $d_2 - d_1 \ll d_2$  and (2) small thickness of the lower layer  $d_1 \ll d_2$ . First consider case (1), which corresponds to the upper liquid layer on the bulk liquid substrate. The dimensional  $k_m$  and  $\tau_m$  are given by

$$\begin{aligned} k_m &= \frac{1}{(d_2 - d_1)^2} \sqrt{\frac{|A_{12g}|}{4\pi\sigma_{\text{eff}}}} \\ \tau_m &= \frac{16(2\pi)^2\sigma_{\text{eff}}\mu_1(d_2 - d_1)^6}{d_1 A_{12g}^2}, \end{aligned} \quad (33)$$

with  $\sigma_{\text{eff}} = \sigma_1\sigma_2/(\sigma_1 + \sigma_2)$ . Note that all variables are in their dimensional form.

Interestingly, the growth time  $\tau_m$  depends only on the viscosity of the lower layer  $\mu_1$  and does not depend on  $\mu_2$ . This can be explained by the fact that the flow in the lower layer which is related to  $\mu_1$ , is much larger than that in the upper one [35]. At constant thickness of the lower layer,  $\tau_m$  is proportional to  $(d_2 - d_1)^6$ , i.e. a liquid film on a bulk liquid substrate evolves faster than the same film on a solid substrate (growth time  $\sim (d_2 - d_1)^5$ ) and even faster than the same film on a solid substrate with slippage (growth time  $\sim (d_2 - d_1)^5/[1 + 3\beta/(d_2 - d_1)]$ ).

In case (2), which corresponds to a liquid film on a solid substrate below a bulk of the other liquid, the dimensional  $k_m$  and  $\tau_m$  are given by:

$$\begin{aligned} k_m &= \frac{1}{d_1^2} \sqrt{\frac{A_{21s}}{4\pi\sigma_1}} \\ \tau_m &= \frac{12(2\pi)^2\sigma_1\mu_1 d_1^5}{A_{21s}^2} \end{aligned} \quad (34)$$

Note that in case (2)  $k_m$  and  $\tau_m$  coincide with  $2\pi/\lambda_{\text{low}}$  and  $\tau_{\text{low}}$ , respectively, where  $\lambda_{\text{low}}$  and  $\tau_{\text{low}}$  are the fastest growing wave length and the growth time of a liquid film below a bulk of the other liquid, calculated from the one-layer theory. This corresponds to a similar result for a Rayleigh-Taylor instability [5, 63].

### E. Long-range apolar and short-range polar interactions

The performed stability analysis based on long-range interactions only, becomes incorrect for mean layer thicknesses in the range of the interaction length  $l$  of an additional short-range interaction. Practically, short-range interactions may become important (well) below 10 nm thickness. In contrast to the exclusive action of the long-range interactions, considered in



section II D, then the stability threshold can be crossed by changing the layer thicknesses  $d_i$ . Fig. 4 shows stability diagrams in the plane spanned by the layer thicknesses for fixed Hamaker constants and different short-range parts of the spreading coefficients  $S_i$ .

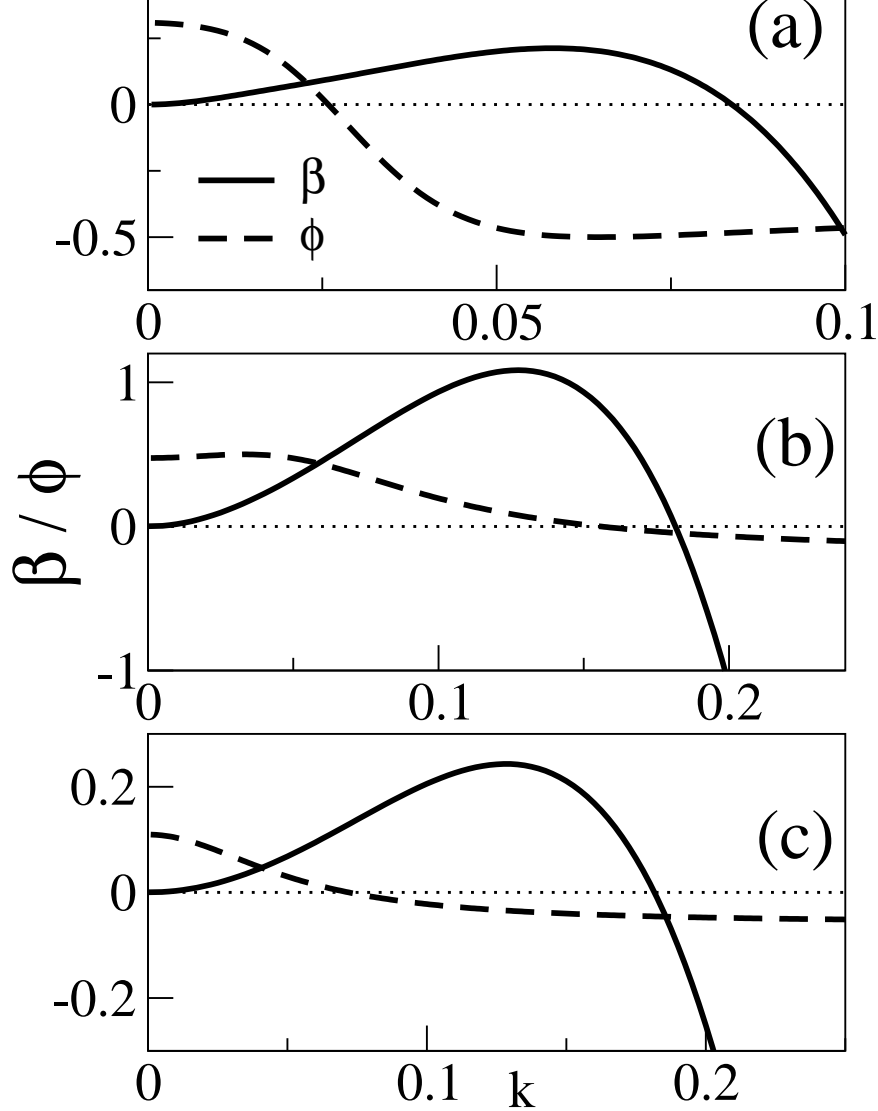


FIG. 4: Different types of stability diagrams in the plane of the layer thicknesses  $(d_1, d_2 - d_1)$ , shown for the strength of the short-range interactions  $S_1$  and  $S_2$  given in the legends. The shaded parts represent linearly stable regions. The Hamaker constants are  $A_{12g} = 1.49$ ,  $A_{21s} = 3.8$ ,  $A_{g21s} = -23.02$ . Panels (a), (b), (c) and (d) correspond to ranges I, III, IV and II in Fig. 5, respectively.

By changing  $S_1$  and  $S_2$  one finds seven topologically different types of such stability diagrams. The regions in the  $(S_1, S_2)$  plane corresponding to the different types are indicated

in Fig. 5. Being in the absolute unstable region in Fig. 5, one can not stabilize the system by changing  $d_1$  or  $d_2$ . This region is bounded on the right by  $(S_1)_{\min} = (e/4)^4 A_{21s}/|A_{12g}|$  and above by  $(S_2)_{\min} = (e/4)^4$ . Only if at least one of the two  $S_i$  is larger than the corresponding critical value, in Fig. 4 a stable region can be found for certain  $(d_1, d_2)$ . If  $S_1 > (S_1)_{\min}$  there exists a stable region that extends towards infinite  $(d_2 - d_1)$ , as shown in Figs. 4(a), (b) and (d). Thereby, for large  $(d_2 - d_1)$  the system is stable for  $(d_1)_{\min} < d_1 < (d_1)_{\max}$ , where  $(d_1)_{\max}$  and  $(d_1)_{\min}$  are the solutions of the equation  $A_{21s}/|A_{12g}| = S_1 x^4 \exp(-x)$ . Similarly, if  $S_2 > (S_2)_{\min}$  there exists a stable region that extends towards infinite  $d_1$ , as in Figs. 4(a) to (d). For large  $d_1$  the system is stable for  $(d_2 - d_1)_{\min} < d_2 < (d_2 - d_1)_{\max}$ , where  $(d_2 - d_1)_{\max}$  and  $(d_2 - d_1)_{\min}$  are the solutions of the equation  $1 = S_2 x^4 \exp(-x)$ . For parameter values in the gray shaded triangle in the center of Fig. 5, one finds additionally a bounded stable region in the  $(d_1, d_2 - d_1)$ -plane, as shown in Figs. 4(b) and (c).

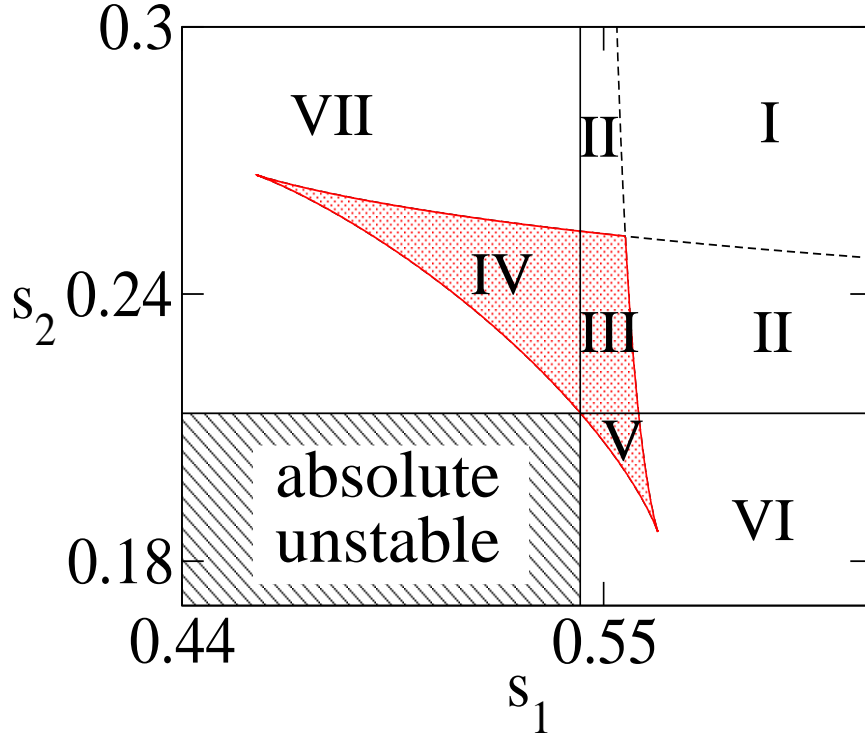


FIG. 5: Phase plane in the variables  $(S_1, S_2)$  of the Si/PMMA/PS/air system. The absolute stable region (hatched rectangle in the lower left corner) is bounded by  $(S_1)_{\min} = (e/4)^4 A_{21s}/|A_{12g}|$  from the right and by  $(S_2)_{\min} = (e/4)^4$  from above. The unstable region is divided into seven subregions, described in the main text.

Combining the different conditions gives the following seven types of stability diagrams.

- I:** The stable region is continuous and extends in respective stripes towards infinite  $d_1$  and  $d_2 - d_1$  (see Fig. 4(a)).
- II:** There exist two separated stable regions, one extending towards infinite  $d_1$  and the other one towards infinite  $d_2 - d_1$  (see Fig. 4(d)).
- III:** Similar to Type II but with an additional bounded stable region (see Fig. 4(b)).
- IV:** A bounded stable region exists together with an unbounded region extending towards infinite  $d_1$  (see Fig. 4(c)).
- V:** Similar to type IV but with the unbounded region extending towards infinite  $(d_2 - d_1)$  (not shown).
- VI:** There exists only one stable region extending towards infinite  $d_1$  (not shown).
- VII:** Similar to type VI but with the unbounded region extending towards infinite  $(d_2 - d_1)$  (not shown).

Further on we will focus our attention on the stability diagram of type I.

## IV. NON-UNIFORM STATIONARY SOLUTIONS

In this section we study the non-uniform stationary solutions of the Eqs. 19 and discuss their stability.

### A. Stationary solutions as extrema of the Lyapunov functional

To find periodic stationary solutions of the scaled Eqs. (19), the time derivatives  $\partial_t h_i$  are set to zero and the equations are integrated to yield

$$\begin{aligned} Q_{11} \partial_x \left( \frac{\delta F}{\delta h_1} \right) + Q_{12} \partial_x \left( \frac{\delta F}{\delta h_2} \right) &= C_1 \\ Q_{21} \partial_x \left( \frac{\delta F}{\delta h_1} \right) + Q_{22} \partial_x \left( \frac{\delta F}{\delta h_2} \right) &= C_2, \end{aligned} \tag{35}$$

where the  $C_i$  are some constants and  $F$  is given by Eq. (27). Note that the l.h.s of Eqs. (35) are the flow in the lower layer and the total flow, respectively. For a stationary state both

flows are zero, i.e. the  $C_1 = C_2 = 0$ . Because the mobility matrix  $\mathbf{Q}$  is non-singular, one concludes from Eqs. (35) that the stationary states of the Eqs. (19) are the extrema of the Lyapunov functional  $F$ , i.e. they are solutions of

$$\begin{aligned} -\partial_{xx}h_1 + \frac{\partial f}{\partial h_1} &= c_1 \\ -\sigma\partial_{xx}h_2 + \frac{\partial f}{\partial h_2} &= c_2, \end{aligned} \tag{36}$$

where  $f$  denotes the local part of Eq. (27) and the constants  $c_i$  correspond to the Lagrangian multipliers introduced in Section II A. To obtain a finite amplitude solution for given mean thicknesses we use continuation techniques [64, 65, 66]. We start with analytically known small-amplitude periodic stationary solutions, which correspond to the linear eigenfunctions for the critical wave number  $k_c$ . By continuation we follow the family of solutions changing the period  $L$ . We characterize the solutions by the deflection amplitudes  $A_1$  and  $A_2$ , the energy  $E$ ,  $L_2 = (1/L) \int [(h_1 - d_1)^2 + (h_2 - d_2)^2] dx$  and the integral mode type  $\phi_{int}$ . To determine the stability of the stationary solutions  $h_i(x)$ , we add small perturbations  $\delta h_i(x) \sim \exp(\beta t)$  to both interfaces  $h_i(x)$ , linearize the full time-dependent evolution equations (19) around  $h_i(x)$  and solve the obtained eigenvalue problem  $\mathbf{L}(h_i, \partial_x h_i, \partial_x) \delta \mathbf{h}(x) = \beta \delta \mathbf{h}(x)$  for the linear operator  $\mathbf{L}$  after discretizing it in space. The sign of the largest eigenvalue  $\beta$  determines the stability of the stationary solution. Note that due to the translational invariance of the evolution equations (19), there exists always a symmetry mode  $\delta h_i(x) = \partial_x h_i(x)$  with the eigenvalue  $\beta = 0$ .

## B. Mode type transitions

### 1. Transition via branch switching

For the Si/PMMA/PS/air system we first chose the parameters  $\mu = \sigma = 1$ ,  $S_1 = S_2 = 1$ ,  $d_1 = 30$ , and  $d_2 = 47$ . We find the primary bifurcation at  $L_c = 2\pi/k_c$  to be subcritical as shown in Fig. 6(a). The stability analysis shows that there exist two stable branches (solid lines) and two unstable branches (dashed lines). Along the first unstable branch, which starts at  $L_c$  and ends at the first saddle-node bifurcation (fold) at  $L \approx 60$  the energy ( $E - E_0$ ) is larger than the energy of the flat films  $E_0$ . It increases as the period decreases, as shown in Fig. 6(b). This branch corresponds to nucleation solutions that have to be overcome to

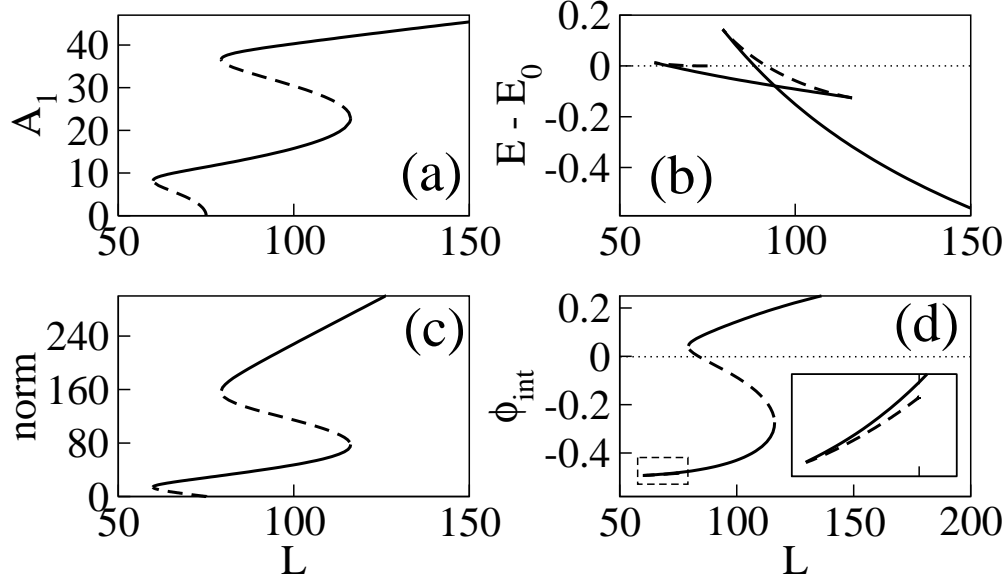


FIG. 6: (a) Amplitude of the lower layer  $A_1$ , (b) relative energy  $E - E_0$ , (c) norm  $L_2$  and (d) integral mode type  $\phi_{int}$  vs. period  $L$  of the stationary periodic solutions, for Si/PMMA/PS/air system with parameters:  $\sigma = 1$ ,  $\mu = 1$ ,  $S_1 = S_2 = 1$ ,  $d_1 = 30$ ,  $d_2 = 47$ . In (d) the inset shows a zoom of the region marked by the dashed box.

break the film in parts smaller than  $L_c$  (see [12] for a discussion of this type of solutions for a one-layer system). The first stable branch starts at the first fold at  $L \approx 59$  and ends at the second fold at  $L \approx 116$ . The corresponding relative energy decreases monotonically with increasing period. For most periods it is less than the energy of the corresponding flat films. The second unstable branch situated between the second fold at  $L \approx 116$  and the third fold at  $L \approx 79$  turns back towards smaller periods. The second stable branch starts at the third fold and goes towards infinite periods. Its energy decreases rapidly from values even above the flat film to values below the ones of the first stable branch. The energy of the second unstable branch is always larger than the energies of the two stable branches. This indicates that it corresponds to nucleation solutions, or critical solutions that have to be overcome to switch between the two stable branches.

The existence of two stable stationary solutions with the period that corresponds to the fastest growing wave length  $\lambda_m$  and with negative relative energy (Fig. 6) allows for a non-trivial behavior during the time evolution. As will be shown in Section V A, during the time evolution different spatial regions can belong to different stable branches, having the same period but different amplitudes and mode types. The two solutions with  $L = \lambda_m$  are shown

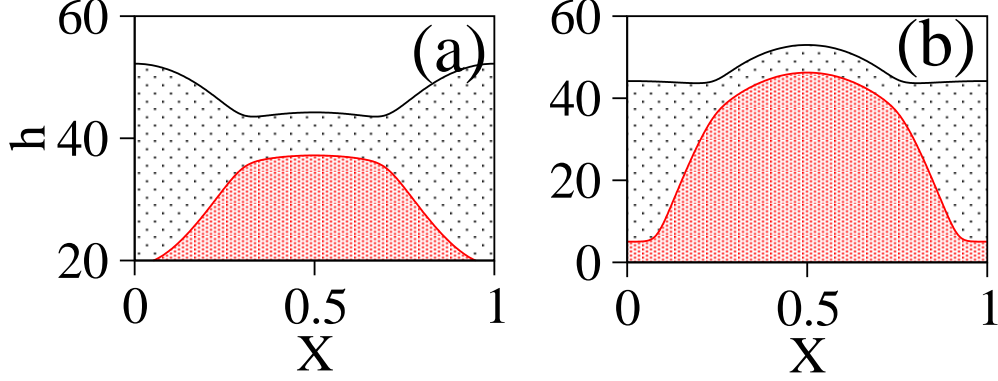


FIG. 7: Stationary solutions, obtained for Si/PMMA/PS/air system with parameters as in Fig. 8 and  $d_1 = 30$ ,  $d_2 = 47$ . (a) the varicose mode with the period  $L = 108.28$  on to the first supercritical branch. (b) the zigzag mode with the same period, on the second supercritical branch. The  $x$  coordinate is scaled with corresponding  $L$ .

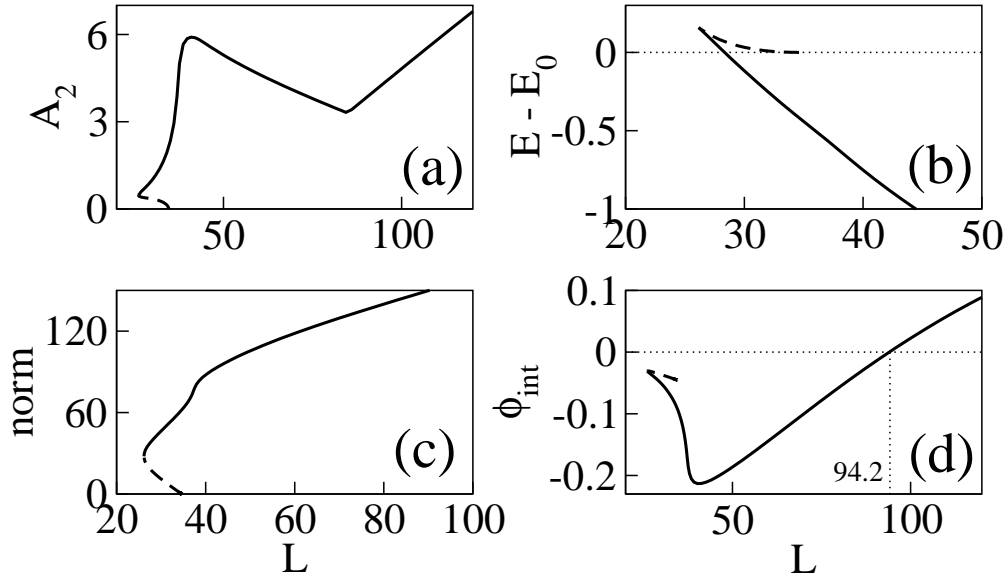


FIG. 8: (a) Amplitude of the upper layer  $A_2$ , (b) relative energy  $E - E_0$ , (c) norm  $L_2$  and (d) integral mode type  $\phi_{int}$  vs. period  $L$  of the stationary periodic solutions, for Si/PMMA/PS/air system with parameters:  $\sigma = 1$ ,  $\mu = 1$ ,  $S_1 = S_2 = 1$ ,  $d_1 = 15$ ,  $d_2 = 40$ .

in Fig. 7. The solution of higher energy (Fig. 7(a)) is of varicose type, whereas the solution of lower energy (Fig. 7(b)) is of zigzag type, as can be seen in Fig. 6(d). A transition between the two solutions is accompanied by a strong increase of the amplitude  $A_1$  (see Fig. 6(a)).

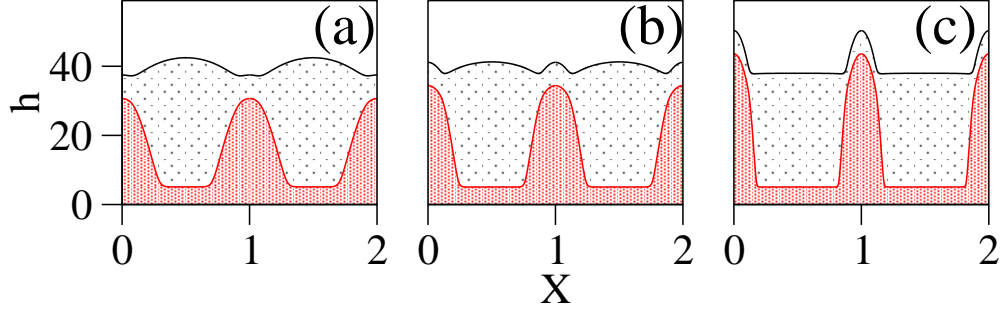


FIG. 9: Stationary solutions for the case of Fig. 6. (a) with fastest growing wave length  $L_a = 50.81$ , (b) with  $L = 84.92$  that corresponds to the minimum of the bifurcation branch in Fig. 6, (c) with  $L = 140$ . For convenience in each case two periods are shown, the  $x$  coordinate is scaled with corresponding  $L$ .

## 2. Transition via coarsening

The mode-type change is not always connected with a transition between different bifurcation branches. Also coarsening along one branch may lead to such a change if the mode-type varies along the branch. For the parameters used in Fig. 8, a varicose mode solution at small periods flips to the zigzag mode solution at large periods. Fig. 8(d) shows that the large amplitude stationary solution corresponding to the fastest growing wave length  $\lambda_m = 50.81$  is of varicose type. This solution is shown in Fig. 9(a), where stationary solutions of different periods are presented for the parameters used in Fig. 8. During coarsening the mean period increases. When it becomes larger than 94.2 (Fig. 8(d)), the solution changes to zigzag type, as shown in Fig. 9(c).

Here we have restricted our attention to a parameter set corresponding to region I of Fig. 5, i.e. corresponding to the stability diagram shown in Fig. 4(a). The existence of a stable branch of stationary solutions which continues towards infinite periods implies that the rupture of the two layers is completely excluded by the short-range repulsion. However, this may not be the case for parameter ranges belonging to other types of stability diagram. A detailed analysis of the stationary solutions for such types will be done elsewhere. In the next Section we test the predictions drawn from the study of stationary solutions by numerically simulating the evolution equations in time.

## V. NONLINEAR TIME EVOLUTION

### A. Change of the mode type

To demonstrate the predicted mode-type transitions in the previous section, we simulate the scaled coupled evolution equations, Eqs. (19), in a one-dimensional domain using both semi-implicit pseudo-spectral and an explicit time integration schemes and periodic boundary conditions. Initial conditions consist of flat layers with an imposed noise of amplitude 0.001. First we chose the parameters as in Fig. 3(a) and Fig. 6. The corresponding time sequence is shown in Fig. 10. The domain length is four times the fastest growing wave length  $\lambda_m$ .  $x$  is scaled by  $\lambda_m$  and time with  $1/\gamma_m$ . In the early stage of evolution the varicose mode is formed ( $t = 5.8$ ). After that the amplitude of the part of the system of the length  $\lambda_m$  increases dramatically and this part (at the boundary of the domain) changes its mode type to the zigzag one ( $t = 7.1$ ). Note that the mode type of the rest of the system remains during this process unchanged. Further on, due to coarsening, the length of the zigzag part of the system increases and the varicose-type drops (in the center of the domain) disappear one by one. The evolution ends when a single drop of the lower layer is left, covered with the upper layer which repeats the form of the liquid-liquid interface. The final state is of the zigzag type.

To demonstrate the mode-type change due to coarsening, we chose the parameters as in Fig. 3(b) and Fig. 8. In the early stage of evolution the deflections of the interfaces are in phase, showing the zigzag mode ( $t = 10.3$ ). But after that, within a very short period of time: from  $t = 10.3$  to  $t = 13.1$ , the mode type changes to the varicose one and the evolution slows down. When the coarsening sets in ( $t = 13.1$ ), the size of the droplets increases ( $t = 263.8$ ,  $t = 636.1$ ) and at very late times ( $t = 733.3$ ), the mode type changes back to the zigzag one. Note that in the considered case, during the change of the mode type, the amplitudes of interfaces do not change dramatically, as in case  $d_1 = 30$ ,  $d_2 = 47$ . In this sense the transition occurs continuously. The mode type transitions, considered above, will be explained in the next section by studying the non-uniform stationary solutions and their stability.

In three dimensions the mode type transition may be related to the change of the surface morphology. As in the one-layer liquid films, driven by various instability mechanisms,



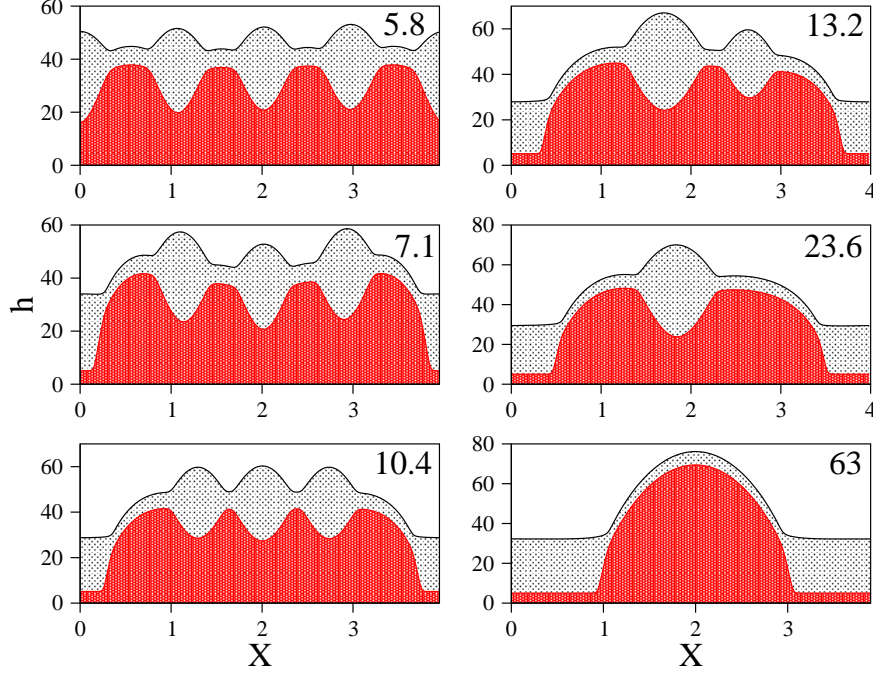


FIG. 10: Time evolution of a Si/PMMA/PS/air system for  $d_1 = 30, d_2 = 47$  and  $S_1 = S_2 = 1, \sigma = 1, \mu = 1$ . The domain length is  $L = 4\lambda_m$ , time is scaled by  $1/\gamma_m$ .

[11, 26, 67], one also expects the same three types of surface morphology in two-layer films: drops, holes and labyrinths. For instance, the varicose-zigzag transition in the early stage of evolution in Fig. 10, may correspond in three dimensions to a hole-drop (drop-hole) transition.

Here we emphasize the difference between the long-time evolution of one-layer and two-layer liquid films. As it was shown in [68], during the process of coarsening the Lyapunov functional  $F$  decreases step-wise with time. Such behavior is explained by passing from one stationary solution with certain period and amplitude to the next one with a larger period and larger amplitude. Important is that both stationary solutions belong to one and the same bifurcation branch, providing the moderate growth of the amplitude. The situation is qualitatively different for two-layer liquid films. The Lyapunov functional  $F$  still decreases monotonically with time, but not anymore step-wise, as shown in Fig. 12(a), where the energy  $F$  is shown vs. time for the case, considered in Fig. 10.

This can be explained by the fact that in the case of the two-layer liquid films a part of the domain can belong to one stable bifurcation branch, whereas the rest of the domain to the other one. Such a composite state is formed between the two energy levels, denoted

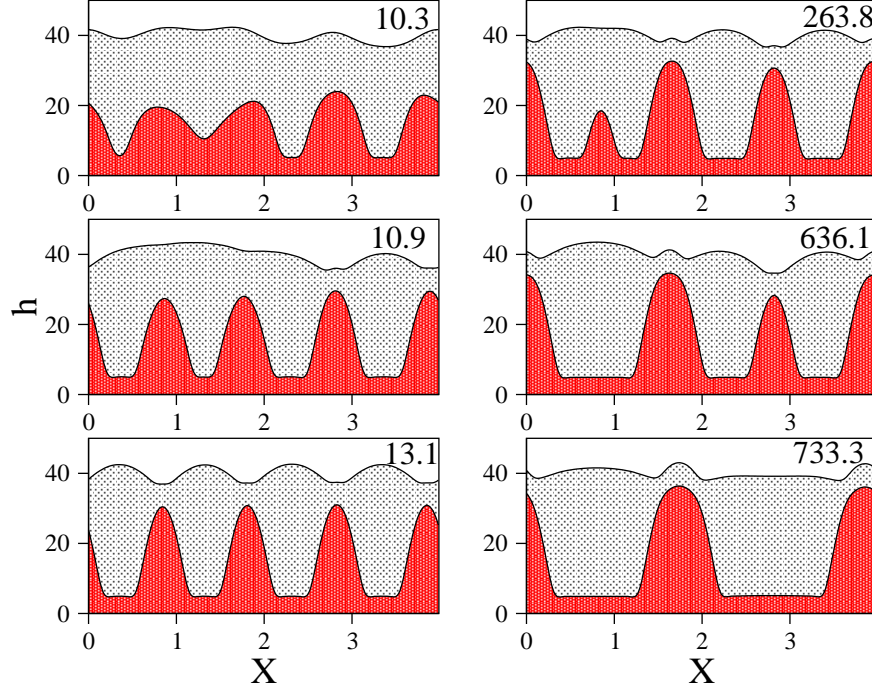


FIG. 11: Time evolution of a Si/PMMA/PS/air system for  $d_1 = 15$ ,  $d_2 = 40$  and  $S_1 = S_2 = 1$ ,  $\sigma = 1$ ,  $\mu = 1$ . The domain length is  $L = 4\lambda_m$ , the time is scaled with  $1/\gamma_m$ .

by the horizontal lines (1) and (2) in Fig. 9(a). Further on, this two parts of the domain evolve separately from each other, explaining the non-step-wise behavior of the Lyapunov functional. The evolution stops when the period becomes equal to the system size.

### B. Large-period stationary solutions

Finally we calculate the possible large-period stationary solutions for different combinations of Hamaker constants. These are shown in Fig. 13 for the case  $S_1 = S_2 = 1$ . For a zigzag mode at large periods the minimal thickness of the upper layer  $h_{\min}^{\text{up}}$  decreases as the period increases. It may become extremely small, as shown for the Si/PMMA/PS/air system at  $d_1 = 30$ ,  $d_2 = 70$ , which would lead to the rupture of the upper layer. This allows to predict the final morphology of the patterns: the liquid-gas interface is quiet flat, with holes, filled up with drops of the lower liquid.

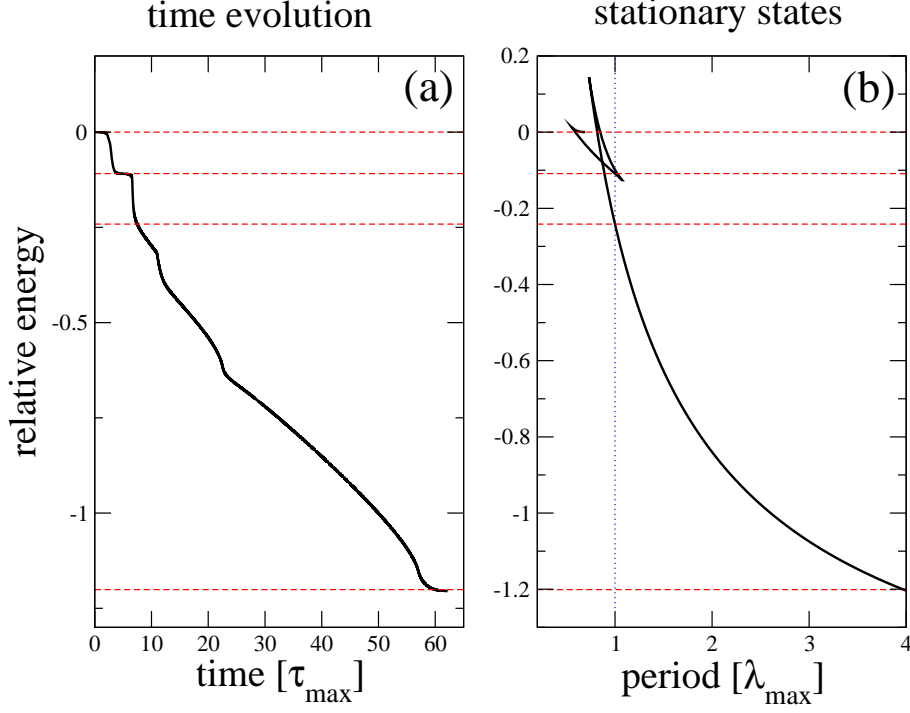


FIG. 12: Relative energy vs. time (a) for evolution of the Si/PMMA/PS/air system with  $d_1 = 30$ ,  $d_2 = 47$ . Relative energy vs. period of the stationary solutions (b). Time is scaled with the characteristic growth time  $\tau_{\max}$  and  $x$  with the fastest growing wave length  $\lambda_{\max}$ . The horizontal lines show the levels of the relative energy 0, the energy of the solution on the first stable branch with the period  $\lambda_m$ , the energy of the solution on the second stable branch with the period  $\lambda_m$  and the energy of the solution with the period  $4 \times \lambda_m$ .

## VI. CONCLUSION

We have derived coupled non-linear evolution equations for the two interface profiles of a two-layer liquid film. We have shown that the two evolution equations can be written in terms of the Lyapunov functional  $F$  which monotonically decreases with time. The stability conditions for the flat films are given in terms of  $F$ . Using these conditions we have shown that the two-layer film is less stable than the effective one-layer films, introduced in Section III B. Even if the both effective one-layer films are stable, the two-layer film may be unstable if the determinant of the energy matrix  $\det \mathbf{E}$  is negative. If the Hamaker constants are given by Eq. (24) and no other forces are present, the stability of the flat films with thicknesses of ( $\sim 100$ ) nm can not be changed by solely changing the thicknesses. In contrast to [35], linear

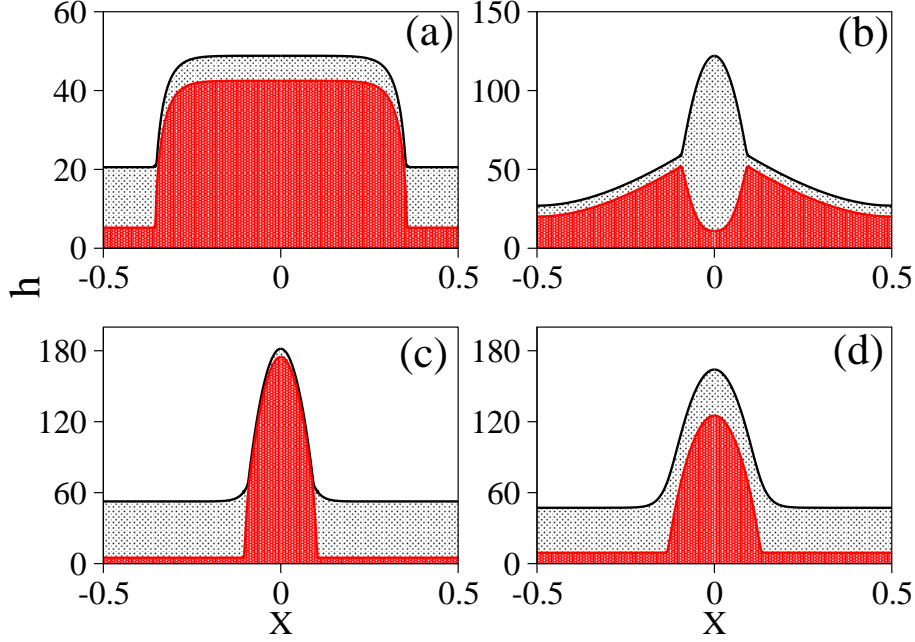


FIG. 13: Large-period stationary states for (a) Si/PMMA/PS/air system with  $d_1 = 30$ ,  $d_2 = 39$ , (b) SiO/PMMA/PS/air with  $d_1 = 30$ ,  $d_2 = 50$ , (c) Si/PMMA/PS/air system with  $d_1 = 30$ ,  $d_2 = 70$ , (d) SiO/PS/PDMS/air with  $d_1 = 30$ ,  $d_2 = 70$ . The rest parameters are:  $\sigma = \mu = 1$ ,  $S_1 = S_2 = 1$ .

stability analysis predicts the varicose as well as the zigzag modes to be primary unstable, depending on the ratio of the layer thicknesses.

To study the long-time evolution we have introduced a stabilizing short-range non Van der Waals interaction. This allows to determine the possible stationary states, which are the extrema of the Lyapunov functional  $F$ . The bifurcation diagrams, obtained for different mean thicknesses  $d_1$ ,  $d_2$  and spreading coefficients  $S_i = 1$ , have a stable branch going towards infinite periods. There exist a non-ruptured stationary states in the long-time limit. The mode-type of the absolute stable solution may change from the small-period varicose to the large-period zigzag on two different ways: (i) via jumping onto a new stable branch and (ii) by following a single stable branch. In case (i) the transition occurs at a certain period. The amplitude of the stationary solution changes dramatically. In the case (ii) the transition occurs continuously without the amplitude jump: small-period varicose mode turns to a large-period zigzag one.

In almost all examples considered here (except for the SiO/PMMA/PS/air system with  $d_1 = 30$ ,  $d_2 = 50$ ), we found a clear zigzag mode to be stable at large periods. A further anal-

ysis of the stationary solutions should show whether or not for the experimentally studied systems [49, 60] with various mean thicknesses  $d_i$ , the large-period zigzag mode is energetically more preferable than the large-period varicose one. Moreover, the detailed analysis of the stationary solutions is required to clarify the questions of the metastability and of the absolute stability of the flat two-layer films. The last issue is especially important for the fabrication of the two-layer homogeneous coating films with thicknesses of 100 nm.

## VII. APPENDIX

Here we rewrite the derivatives  $\partial_x \sigma_{12}$  and  $\partial_x \sigma_2$  in terms of the gradients of the local thicknesses  $\partial_x h_i$ , taking into account thermocapillarity.

In the long-wave approximation the temperature field in both layers is a linear function of the vertical coordinate  $z$  [4]  $T_i = a_i z + b_i$ . For completeness we consider here a three-layer geometry, taking also a gas layer of finite thickness  $d_g = d_t - d_2$  into account, where  $d_t$  is the distance between the substrate and the upper plate, as shown in Fig. 14. The temperature in the gas layer is  $T_g = a_g z + b_g$ . The boundary conditions at both interfaces are continuity of the temperature field and Newton's cooling law  $\kappa_i \partial_z T_i = \kappa_k \partial_z T_k$ , where  $\kappa_i$  is the thermal conductivity of the  $i$ -th layer. The temperatures at the substrate  $T_0$  and at the upper plate  $T_t$  are constant.

The coefficients  $a_i$  and  $b_i$  depend on the local thicknesses  $h_i$  and are given by

$$a_g = \frac{\alpha \Delta T}{d_t - h_2 + \frac{\kappa_g}{\kappa_1} h_1 + \frac{\kappa_g}{\kappa_2} (h_2 - h_1)}$$

$$a_2 = \frac{a_g \kappa_g}{\kappa_2}, \quad a_1 = \frac{a_g \kappa_g}{\kappa_1}$$

$$b_1 = T_0, \quad b_g = T_t - a_g d_t$$

$$b_2 = a_g \kappa_g h_1 \left( \frac{1}{\kappa_1} - \frac{1}{\kappa_2} \right) + T_0,$$

where  $\Delta T = T_0 - T_2$  and

$$\alpha = \frac{d_2 - d_t - \kappa_g h_1 / \kappa_1 - \kappa_g (d_2 - d_1) / \kappa_2}{\kappa_g h_1 / \kappa_1 - \kappa_g (d_2 - d_1) / \kappa_2}.$$

Here  $T_2$  is the temperature of the liquid-gas interface, when both interfaces are undeformed, i.e. for  $h_i = d_i$ .

The above formulas allow to determine the derivatives  $\partial_x \sigma_{12}$ ,  $\partial_x \sigma_2$

$$\partial_x \sigma_{12} = \Gamma_{11} \partial_x h_1 + \Gamma_{12} \partial_x h_2 \tag{37}$$

$$\partial_x \sigma_2 = \Gamma_{21} \partial_x h_1 + \Gamma_{22} \partial_x h_2,$$

where the matrix  $\mathbf{\Gamma}$  is determined as follows

$$\mathbf{\Gamma} = a \begin{pmatrix} \frac{\kappa_g}{\kappa_1} \frac{d\sigma_1}{dT} b & -\frac{\kappa_g}{\kappa_1} \frac{d\sigma_1}{dT} h_1 \left( \frac{\kappa_g}{\kappa_2} - 1 \right) \\ \frac{d\sigma_2}{dT} (bc - \frac{\kappa_g}{\kappa_2} h_2 b) & \frac{d\sigma_2}{dT} \left\{ \frac{\kappa_g}{\kappa_2} (d_t + h_1 b) - b h_1 \left( \frac{\kappa_g}{\kappa_2} - 1 \right) \right\} \end{pmatrix} \tag{38}$$

Here  $a = (\alpha\Delta T)/\left[d_t - h_2 + \frac{\kappa_g}{\kappa_1}h_1 + \frac{\kappa_g}{\kappa_2}(h_2 - h_1)\right]^2$ ,  $b = \kappa_g(1/\kappa_1 - 1/\kappa_2)$  and  $c = \{d_t - h_2(1 - \frac{\kappa_g}{\kappa_2})\}$ .

For the linear normal Marangoni effect  $d\sigma_{12}/dT$  and  $d\sigma_2/dT$  are negative and constant. The equations Eqs. 38 should be used in Eqs. 19 to obtain the closed system of equations for  $h_1$  and  $h_2$ .

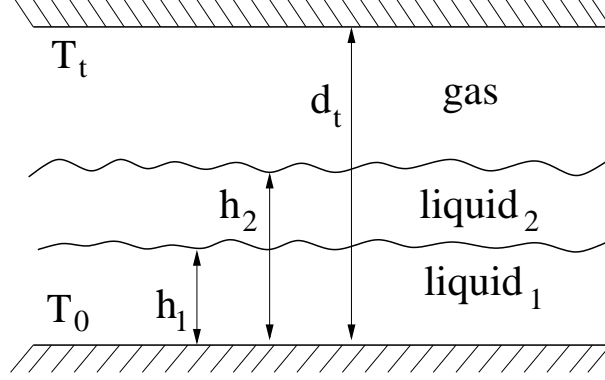


FIG. 14: Sketch of the system with a finite thickness of the gas layer:  $d_g = d_t - d_2$ .

- 
- [1] O. Reynolds, Phil. Trans. Roy. Soc. **177**, 157 (1886).
  - [2] A. Sommerfeld, Z. Math. Phys. **50**, 97 (1904).
  - [3] D. Dowson, *History of Tribology* (Longmans, Green, 1979).
  - [4] A. Oron, S. H. Davis, and S. G. Bankoff, Rev. Mod. Phys. **69**, 931 (1997).
  - [5] S. G. Yiantsios and B. G. Higgins, Phys. Fluids A **1**, 1484 (1989).
  - [6] A. Oron and P. Rosenau, J. Physique II France **2**, 131 (1992).
  - [7] V. S. Mitlin, J. Colloid Interface Sci. **156**, 491 (1993).
  - [8] E. Ruckenstein and R. K. Jain, J. Chem. Soc. Faraday Trans. II **70**, 132 (1974).
  - [9] M. B. Williams and S. H. Davis, J. Colloid Interface Sci. **90**, 220 (1982).
  - [10] P. G. de Gennes, Rev. Mod. Phys. **57**, 827 (1985).
  - [11] A. Sharma and R. Khanna, Phys. Rev. Lett. **81**, 3463 (1998).
  - [12] U. Thiele, K. Neuffer, Y. Pomeau, and M. G. Velarde, Colloid Surf. A **206**, 135 (2002).
  - [13] U. Thiele, M. G. Velarde, and K. Neuffer, Phys. Rev. Lett. **87**, 016104 (2001).
  - [14] A. Sharma, Langmuir **9**, 861 (1993).
  - [15] A. Sharma, Langmuir **9**, 3580 (1993).
  - [16] U. Thiele, Eur. Phys. J. E **12**, 409 (2003).
  - [17] A. L. Bertozzi, G. Grün, and T. P. Witelski, Nonlinearity **14**, 1569 (2001).
  - [18] U. Thiele and E. Knobloch, Physica D **190**, 213 (2004).
  - [19] E. Schäffer and U. Steiner, Eur. Phys. J. E **8**, 347 (2002).
  - [20] G. Reiter, Phys. Rev. Lett. **68**, 75 (1992).
  - [21] G. Reiter, Langmuir **9**, 1344 (1993).
  - [22] K. Jacobs, R. Seemann, G. Schatz, and S. Herminghaus, Langmuir **14**, 4961 (1998).
  - [23] S. J. VanHook, M. F. Schatz, W. D. McCormick, J. B. Swift, and H. L. Swinney, Phys. Rev. Lett. **75**, 4397 (1995).
  - [24] R. Seemann, S. Herminghaus, and K. Jacobs, Phys. Rev. Lett. **86**, 5534 (2001).
  - [25] A. Sharma and G. Reiter, J. Colloid Interface Sci. **178**, 383 (1996).
  - [26] M. Bestehorn, A. Pototsky, and U. Thiele, Eur. Phys. J. B **33**, 457 (2003).
  - [27] A. A. Golovin, A. A. Nepomnyashchy, and L. M. Pismen, Phys. Fluids **6**, 34 (1994).
  - [28] G. Reiter, A. Sharma, A. Casoli, M.-O. David, R. Khanna, and P. Auroy, Langmuir **15**, 2551



- (1999).
- [29] K. Jacobs, S. Herminghaus, and G. Schatz, Phys. Rev. Lett. (1997), submitted 8/97.
  - [30] C. J. V. Oss, M. K. Chaudhury, and R. J. Good, Chem. Rev. **88**, 927 (1988).
  - [31] R. Seemann, S. Herminghaus, and K. Jacobs, J. Phys.-Cond. Mat. **13**, 4925 (2001).
  - [32] Z. Q. Lin, T. Kerle, S. M. Baker, D. A. Hoagland, E. Schäffer, U. Steiner, and T. P. Russell, J. Chem. Phys. **114**, 2377 (2001).
  - [33] Z. Q. Lin, T. Kerle, T. P. Russell, E. Schäffer, and U. Steiner, Macromolecules **35**, 3971 (2002).
  - [34] D. Merkt, A. Pototsky, M. Bestehorn, and U. Thiele, Phys. Fluids **submitted** (2004).
  - [35] F. Brochard-Wyart, P. Martin, and C. Redon, Langmuir **9**, 3682 (1993).
  - [36] K. D. Danov, V. N. Paunov, N. Alleborn, H. Raszillier, and F. Durst, Chem. Eng. Sci. **53**, 2809 (1998).
  - [37] K. D. Danov, V. N. Paunov, S. D. Stoyanov, N. Alleborn, H. Raszillier, and F. Durst, Chem. Eng. Sci. **53**, 2823 (1998).
  - [38] V. N. Paunov, K. D. Danov, N. Alleborn, H. Raszillier, and F. Durst, Chem. Eng. Sci. **53**, 2839 (1998).
  - [39] D. Bandyopadhyay, *Stability and dynamics of bilayers* (2001), master-thesis, Dep. Chem. Eng., Ind. Inst. Tech. Kanpur.
  - [40] A. Pototsky, M. Bestehorn, D. Merkt, and U. Thiele, Phys. Rev. E **70**, 025201(R) (2004).
  - [41] Y. L. Zhang, O. K. Matar, and R. V. Craster, J. Colloid Interface Sci. **262**, 130 (2003).
  - [42] R. V. Craster and O. K. Matar, J. Fluid Mech. **425**, 235 (2000).
  - [43] O. K. Matar, R. V. Craster, and M. R. E. Warner, J. Fluid Mech. **466**, 85 (2002).
  - [44] C. Renger, P. Müller-Buschbaum, M. Stamm, and G. Hinrichsen, Macromolecules **33**, 8388 (2000).
  - [45] O. Wunnicke, P. Müller-Buschbaum, M. Wolkenhauer, C. Lorenz-Haas, R. Cubitt, V. Leiner, and M. Stamm, Langmuir **19**, 8511 (2003).
  - [46] M. D. Morariu, E. Schäffer, and U. Steiner, Phys. Rev. Lett. **92**, 156102 (2004).
  - [47] A. Faldi, R. J. Composto, and K. I. Winey, Langmuir **11**, 4855 (1995).
  - [48] P. Lambooy, K. C. Phelan, O. Haugg, and G. Krausch, Phys. Rev. Lett. **76**, 1110 (1996).
  - [49] Q. Pan, K. I. Winey, H. H. Hu, and R. J. Composto, Langmuir **13**, 1758 (1997).
  - [50] P. Martin, A. Buguin, and F. Brochard-Wyart, Europhys. Lett. **28**, 421 (1994).

- [51] J. N. Israelachvili, *Intermolecular and Surface Forces* (Academic Press, London, 1992).
- [52] A. A. Nepomnyashchii and I. B. Simanovskii, *Pmm-J. Appl. Math. Mech.* **54**, 490 (1990).
- [53] A. A. Nepomnyashchii and I. B. Simanovskii, *Q. J. Mech. Appl. Math.* **50**, 149 (1997).
- [54] G. F. Teletzke, H. T. Davis, and L. E. Scriven, *Rev. Phys. Appl.* **23**, 989 (1988).
- [55] R. M. Pasley, *J. Colloid Interface Sci.* **84**, 531 (1981), BESORGEN!
- [56] B. V. Deryagin and L. D. Landau, *Acta Physicochim.* **14**, 633 (1941).
- [57] E. J. W. Verwey and J. T. G. Overbeck, *Theory of the Stability of Lyophilic Colloids* (Elsevier, Amsterdam, 1948).
- [58] H. Ohshima, *Colloid Polym. Sci.* **252**, 158, 257 (1974), BESORGEN!
- [59] E. S. Manteuffel and K. Vetter, *Lineare Algebra* (Teubner Verlagsgesellschaft, Leipzig, 1972).
- [60] M. D. Morariu, E. Schäffer, and U. Steiner, *Eur. Phys. J. E* **12**, 375 (2003).
- [61] M. O. David, G. Reiter, T. Sitthai, and J. Schultz, *Langmuir* **14**, 5667 (1998).
- [62] M. Sferazza, C. Xiao, R. A. L. Jones, D. G. Bucknall, J. Webster, and J. Penfold, *Phys. Rev. Lett.* **78**, 3693 (1997).
- [63] S. G. Yiantsios and B. G. Higgins, *J. Colloid Interface Sci.* **147**, 341 (1991).
- [64] E. Doedel, H. B. Keller, and J. P. Kernevez, *Int. J. Bif. Chaos* **1**, 493 (1991).
- [65] E. Doedel, H. B. Keller, and J. P. Kernevez, *Int. J. Bif. Chaos* **1**, 745 (1991).
- [66] E. Doedel, A. Champneys, T. Fairfrieve, Y. Kusnetzov, B. Sandstede, and X. Wang, *Continuation and Bifurcation Software for Ordinary Differential Equations* (Concordia University, Montreal, 1997).
- [67] M. Bestehorn and K. Neuffer, *Phys. Rev. Lett.* **87**, 046101,1 (2001).
- [68] U. Thiele, L. Brusch, M. Bestehorn, and M. Bär, *Eur. Phys. J. E* **11**, 255 (2003).